Assessing Tissue Damage Around a Tape Spring Steerable Needle With Sharp Turn Radii

Omar T. Abdoun and Mark Yim, *Member, IEEE*

***Abstract*—Steerable needles are a novel technology that offers a wide range of uses in medical diagnostics and therapeutics. Currently, there exist several steerable needle designs in the literature, however, they are limited in their use by the number of possible turns, turn radius, and tissue damage. We introduce a novel design of a tape spring steerable needle, capable of multiple turns, that minimizes tissue damage. In this study, we measure the turning radius of our steerable needle in porcine liver tissue in vitro with ultrasound and estimate tissue damage in gel blocks using image analysis and 3D plaster casting. We were able to demonstrate our steerable needle's ability to steer through biological tissue, as well as introduce a novel method for estimating tissue damage. Our findings show that our needle design showed lower damage compared to similar designs in literature, as well as tissue stiffness being a protective factor against tissue damage.**

***Index Terms*—Interventional radiology, minimally invasive, steerable catheter, steerable needle, tape spring.**

***Impact Statement*—In this work we demonstrate a new method to estimate needle tissue damage and use that to show that a tape spring steerable needle imparts minimal surrounding tissue damage while steering.**

I. Introduction

STEERABLE needles are a technology that could dramatically improve the accuracy and reach of minimally invasive medical interventions. These procedures include biopsies, ablations, targeted drug deliveries, cyst drainage, among many others [1]. While conventional needles and probes are generally limited to targets that are accessible via a straight trajectory, steerable needles can create trajectories that avoid anatomical obstacles and sensitive regions by curving around them. Robotic approaches to creating steerable needles has had significant attention from the medical robotics community [2], [3].

Manuscript received 26 May 2023; revised 15 October 2023 and 14 December 2023; accepted 14 December 2023. Date of publication 17 January 2024; date of current version 23 February 2024. The work of Omar Abdoun was supported by NIH Medical Scientist Training Program under Grant T32 GM07170. This work was supported by NSF STTR under Grant 1746583. The review of this article was arranged by Editor Paolo Bonato. *(Corresponding author: Mark Yim.)*

Omar T. Abdoun is with the Department of Bioengineering and The Perelman School of Medicine, University of Pennsylvania, Philadelphia, PA 19104 USA (e-mail: omar.abdoun@pennmedicine.upenn.edu).

Mark Yim is with the Department of Mechanical Engineering and Applied Mechanics, University of Pennsylvania, Philadelphia, PA 19104 USA (e-mail: yim@seas.upenn.edu).

Digital Object Identifier 10.1109/OJEMB.2024.3355286

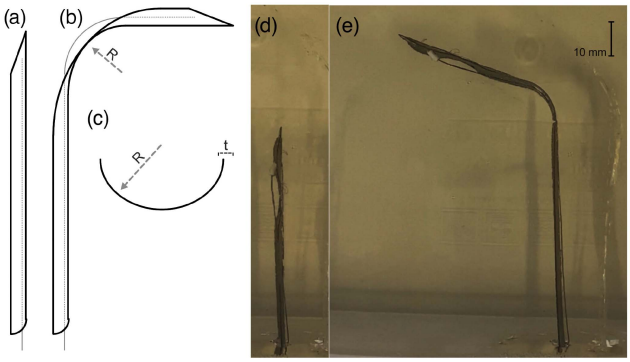

Fig. 1. (a) A schematic of a straight tape spring needle and (b) one with an induced bend with R turn radius. (c) A schematic of a head-on view of a needle with thickness t, with R the transverse radius of curvature of the tape spring. (d) A straight, unbent tape spring needle and (e) one with an induced bend.

Research in steerable needles has yielded four main areas of focus toward devices for clinical use: 1) mechanics-based modeling, 2) planning in 3D with uncertainty, 3) human in the loop control, and, 4) minimizing radius of curvature. In a previous study [4], we introduced a proof of concept for a novel steerable needle addressing these categories. The mechanism behind our approach is the use of a cable driven tape spring as the body of the steerable needle.

Tape springs have the advantage of high axial stiffness, which allows for penetration into tissue when they are straight, yet they can also be reversibly buckled to enact a turn [5]. The bending stiffness at this buckled portion is low and allows the direction of the needle to be altered with ease. In addition, minimal force is required to propagate an existing bend along the body of the needle allowing the head of the needle to carve a path that the body follows.

In the previous work [4], we showed that the turning radius for the tape spring steerable needle (shown in Fig. 1) is consistent and independent of the tissue stiffness, simplifying steering. The needle-tissue forces were modeled, making for predictable guidance inputs and behavior. This turning radius is the smallest of any steerable needle in the literature.

Reducing the turning radius has been a goal for a variety of steerable needle approaches [6] both for better control of

(a) (b) (c)

Fig. 2. Image overlay illustrating area shift as the needle is inserted. Images (a) and (b) show the two stages of the needle path. Image (c) shows the paths of the two needles overlaid with the area shift highlighted in red and the maximum perpendicular distance shown in green.

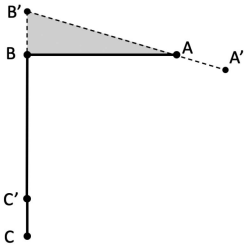

Fig. 3. Maximum normal tissue stress model where initial needle position is defined by ABC and shifted tissue position is defined by $A'B'C'$.

the device, as well as reducing tissue damage as tissue damage from some steerable needle approaches can be especially problematic [7], [8].

The liver is one of the most common sites of metastatic spread from cancers originating in other organs. The liver is a highly vascular organ that partially resides behind the ribs. These factors make access to the right upper lobe of the liver difficult with straight devices. In this paper we show a critical step in proving the feasibility of steerable needle for patient care use in real organ tissues. In addition, minimizing damage to surrounding tissues is an important factor and we present a novel method to quantify tissue damage that occurs from needle use.

II. Materials and Methods

A. Characterizing Tissue Displacement and Tissue Stress

For tissue damage, the most reasonable optimal case would be no damage beyond the space occupied by the needle itself.

On the other hand, an inserted straight needle that then curves in place will tear an arc of tissue as it bends. In our case, the curving path is created as the needle is advanced such that it minimizes tearing through adjacent tissue.

To minimize tissue damage from turns, the normal reaction stress needed to maintain the location of a turn should not exceed the failure stress of the surrounding tissue. Thus, minimizing the reaction stress from the tissue will help to reduce damage and also reduce the effect of inhomogeneous tissue that might cause the needle to steer in unexpected ways. To achieve both minimal damage and good positional accuracy, we conducted a set of experiments that tracked the displacement of needle turns while simultaneously measuring the needle insertion force to estimate reaction stresses.

Here, the same steerable needle makes a single turn in trials with 7 kPa, 13 kPa, and 36 kPa stiffness gels. Video captures the needle being pushed into the gels while the insertion force is measured simultaneously. Photo editing software traced the outline of each needle on images at multiple time points of each run. Each of these images is overlaid on the first frame of that trial to determine any deflections of the needle and infer measurements of stress on the tissue.

Fig. 2 shows an example overlay image. Black dashes indicate distances 10 mm apart. The outline in the initial position is pictured in Fig. 2(a), and the deeper position in Fig. 2(b). Fig. 2(c) combines the two highlighting the difference in red. The maximum distance between the two lines is recorded as the maximum linear displacement. The "X" marker seen to the left is a fiducial marker used to line up images. For each overlay image, both the maximum distance (green line) and area (red highlight) between the initial and deeper image perpendicular to the initial trajectory were recorded. Maximum normal tissue stress was then estimated using the model in Fig. 3. In this simple model, we make a first-order approximation of the upper bound for the stress. The curved bend in the needle is simplified to a single hinge point. In Fig. 3, A represents the needle tip, B represents the hinge joint in the model prior to displacement, B' represents the hinge joint after displacement, C represents the proximal end of the needle prior to displacement, and C' represents the proximal end of the needle after displacement. Segment ABC represents the initial position of the needle and segment A'B'C' represents the needle after the displacement.

The length of the horizontal segment BA in Fig. 3 is set to be the minimum horizontal needle length after a turn has been made. The tissue displacement profile is also assumed to decrease linearly to zero at the tip of the needle based on previously observed small needle tip displacements. The maximum measured input force for the smallest horizontal needle segment length in a particular gel stiffness is the input force used to calculate the stress. Coincidentally, under this simplified model, the grey region also represents the stress profile of the model as the stress is proportional to the displacement (maximum at the hinge B' and 0 at the tip A'). Ideally, the maximum stress at B' does not exceed values that will damage tissue. For example, the average failure stress for human liver in tensile loading is between 40 kPa and 60 kPa [9].

B. Tissue Damage Measurement

Dye injection into the path that a needle carves in a tissue phantom has been used previously to qualitatively assess the relative amount of damage caused by steering needles [7]. To assess tissue damage of our prototype steerable needle, we build on this by injecting Alja-Safe alginate casting material into each needle path and measuring the mass of each cast as a surrogate for damage volume. Thus, instead of a 2D approximation (using dye) of 3D damage, we get a better 3D metric for the damage. In this experiment, we perform successive needle insertions into a gel tissue phantom with an 11 gauge needle, 11 gauge coring biopsy needle, our prototype steerable needle with a straight trajectory, and our prototype needle with a turn in the trajectory.

Each needle was inserted into the test material to a depth of 9 cm for 5 successive trials each and a turn was performed with our device at 5 cm depth. The casting material was then injected into the needle path using a smaller, 18 gauge blunt needle to avoid damaging surrounding tissue and affecting the tissue damage measurement. After the casts were set, the gel was removed by melting the gelatin, and the mass of each cast was measured. These casts retained the shape of the path carved by each test needle in the gel even after the surrounding gel was removed. In a few cases, casting material was injected too quickly and the material damaged the needle path. These failed trials were removed before a mass was measured if the casting material appeared to tear surrounding tissue. The viscosity of the alginate casting material was low enough that with slow injections, minimal to no deflection was apparent from injections that were included in the analysis.

C. Ultrasound Testing

The tape spring steerable needle was inserted into whole porcine liver fixed in gelatin for stability under ultrasound guidance. The linear ultrasound was used and set to thyroid mode in order to improve contrast and visibility of the needle. The needle was inserted until the tip was 1 cm above the inferior aspect of the liver and a turn was performed. An image of the needle turn in the liver is presented in Fig. 6.

III. Results

A. Characterizing Tissue Displacement and Tissue Stress

Results of the displacement test can be seen in Fig. 4 where results from 7 kPa, 13 kPa, and 36 kPa gels are represented by green, blue, and magenta symbols, respectively. Fig. 4(a) shows displacement areas plotted against insertion force and maximum linear displacement in Fig. 4(b).

In our previous work [4], the insertion force was shown to be linearly correlated with the depth of the needle insertion. In Fig. 4 sequential points going deeper into the tissue for a given trial run correspond with larger forces.

The maximum linear displacements at about 1 N in the 36 kPa and 13 kPa trials were 1.3 mm and 3.9 mm, respectively. No forces were recorded to reach 1 N for any of the 7 kPa trials. At 334 mN, the maximum force reached for 7 kPa, the maximum single linear displacement measured was 4.5 mm.

B. Tissue Damage Measurement

Masses of alginate casts of needle paths made in 13 k kPa tissue phantoms are presented in Fig. 5. Error bars represent standard deviations for cast masses over 5-6 trials for each needle type.

C. Ultrasound Testing

Ultrasound visualization of the steerable needle prototype with a single bend performed in porcine liver. The turn radius

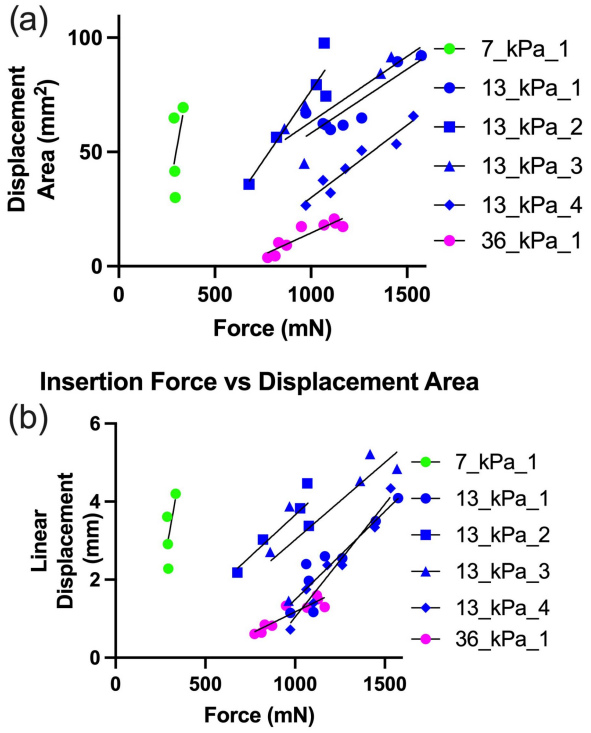

Fig. 4. (a) Needle insertion force vs displacement area across varying gel stiffness. (b) Needle insertion force vs maximum linear displacement across varying gel stiffness.

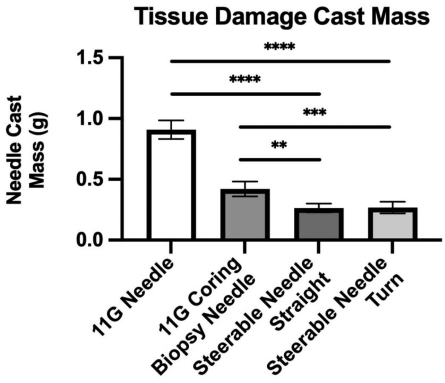

Fig. 5. Needle path cast masses for each set of needle paths tested. $^{**}P \leq 0.01$, $^{***}P \leq 0.001$, $^{****}P \leq 0.0001$.

pictured is 7.9 mm, and the smallest turn radius achieved using our device in liver tissue is 3.3 mm.

IV. Discussion

A. Characterizing Tissue Displacement and Tissue Stress

The slopes of the insertion force vs. displacement area trials show a general negative correlation with the stiffness of the surrounding material. Displacement area has been used to measure tissue damage due to needle insertions in the past [10] and these results indicate that higher stiffness tissues may be less susceptible to damage due to needle insertion. In addition, that the

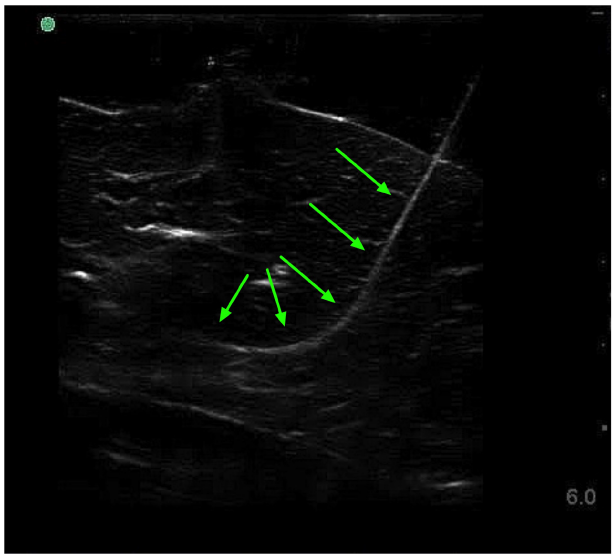

Fig. 6. Steerable Needle visualized using ultrasound in porcine liver. Green arrows point to "L" shaped white line near the center of the image representing the steerable needle with a turn engaged. Scale bar on the right with 1 cm between each dash.

plots for displacement area and maximum linear displacement are nearly identical verifies what one would expect for the linear stress model (Fig. 3).

It is interesting to note that the freehand accuracy error, distance from the target, for freehand percutaneous needle placements is approximately 16 mm [11]. This is larger than all turn displacements measured in this study as seen in Fig. 4(b), even in the worst case displacement, 4.5 mm for compliant 7 kPa gel.

In all trials, the angle between the proximal and distal straight sections of the needle changed throughout the trial with the rotation being in line with the direction of the tissue normal reaction force. This angle change can be seen in Fig. 2. While these experiments were designed to be performed without active steering so that we could evaluate the natural tendency of the needle with a turn subjected to an insertion force, the needle direction can be changed at any time. This means that the potential accuracy error that could be introduced from the turn displacement is theoretically smaller than errors that are already experienced by the standard of care for needle placement. In actual use, the steered direction of the tip of this device allows the user to counteract the tendency for the needle angle to change and increases the theoretical accuracy of the device as the angle of approach towards a target and does not depend as heavily on the insertion trajectory as is the case with conventional approaches [11].

Table I shows the calculated maximum tissue normal reaction stress based on the model shown in Fig. 3. The calculated maximum stress, 19.5 kPa, did not exceed average failure stress of human liver (40 kPa - 61 kPa) as characterized by Kemper et al. [9]. Given that insertion velocity is proportional to cutting force [12], decreasing the insertion velocity can be a method used to minimize the cutting force and therefore, the insertion force and the resulting normal tissue reaction stress and the turn displacement as discussed in our previous work [4].

TABLE I
CALCULATED MAX TISSUE NORMAL STRESS

Gel Stiffness	Maximum Force (mN)	Horizontal distance (mm)	Max Normal reaction Stress (kPa)
7 kPa	449	22.5	7.96
13 kPa	1236	25.5	19.46
36 kPa	949	22	17.25

B. Tissue Damage Measurement

Fig. 5 shows each device's average measured cast mass. Here we demonstrate the ability of our tissue damage measurement method based on the amount of tissue that they displace while being inserted into a tissue phantom. While the dye injection method used by Swaney et al. [7] yields a qualitative comparison between different needle paths or images that could be analyzed in two dimensions, our new method yields a quantitative result that accounts for tissue damage in three dimensions. This method is useful to guide the design process for minimizing potential damage to surrounding tissue and hemorrhage prior to in vivo testing on animals or humans. Tissue damage analysis was performed in gel tissue phantoms in place of real tissues since the gels are transparent, which makes knowing when to stop injecting casting material more straightforward. In addition, isolating the casting material was easily achieved by melting the gel instead of careful dissection, as would be required with real tissue. Finally, the heterogeneous nature of real tissue, such as small vessels that could act as a sink for the injected casting material could lead to inconsistent measurements. However, in the future, adapting this volumetric tissue damage measurement to real tissues could prove to be useful.

Measured tissue damage was significantly lower using our prototype tape spring steerable needle than both the conventional 11 G needles which are of a similar diameter as our needle. Since the tape spring device only has a semicircular cross-section (or even a smaller subtended angle than 180 degrees), we hypothesize that this lesser tissue damage is due to the slimmer cross-sectional area of our device which occupies a relatively smaller volume, as compared to a conventional needle which has a circular cross-section. Fig. 5 also shows that performing a turn in the needle path did not significantly increase the measured tissue damage of the tape spring device as compared to a straight trajectory. While surrounding tissue damage has been a pitfall of other steerable needle designs, based on these results, the tape spring mechanism could prove to be a practical one that minimizes adjacent tissue injury, and consequently complications due to hemorrhage.

C. Ultrasound Testing

Here we demonstrate in an ultrasound experiment the ease of visualization of the steerable needle under ultrasound guidance in biological tissue, achieving an important step in approaching clinical use. In addition, we show that we are able to perform

a turn in porcine liver. Both of these results indicate that our prototype has the potential to be of clinical utility as it is capable of turns in porcine liver and can be easily visualized using a common imaging modality. Our device is capable of small turn radii that are consistent with their performance in tissue phantoms in our previous work. These small turn radii, as small as 3.3 mm are the smallest turn radii that a steerable device is capable of performing in real tissue [4].

V. Conclusion

What we can see from Fig. 4 is that tissue stiffness is protective against tissue damage. An implication of this result is that certain tissues may be better suited for this specific design. Namely, this needle may be better utilized in liver than in the brain which is a much more compliant organ. Alternatively, a subject of future exploration could be to modify the needle to require smaller forces and match a specific design to specific applications in more compliant tissues. Minimizing insertion forces decreases tissue displacement area, and therefore tissue damage, which can be done by decreasing velocity or optimizing tip geometry.

Overall linear displacements are small relative to freehand placement error, even for passive turns. This bodes well for the potential increase in needle placement accuracy that could be afforded using a tape spring steerable needle. The turn displacement would also be even smaller under active steering rather than the passive steering used in the experiments.

The stresses in tissue phantoms don't exceed the failure stress of the human liver in our tissue stress experiment. Adjacent tissue stress is the causative factor for tissue damage, meaning that this design could be feasibly used to steer in biological tissues without excessive tissue damage and accompanying complications. As tissue damage is a major factor that affects the feasibility of using steerable needles to navigate solid organs, low tissue stresses are a major advantage of the tape spring steerable needle design.

Here we presented a new method of in vitro tissue damage estimation. This method could be used to iterate/optimize surgical devices, such as ours, or others before use in live subjects. This could help minimize the likelihood of failure of surgical device designs due to tissue damage/hemorrhage when tested in live subjects.

Our Steerable needle showed low measured tissue damage relative to similarly sized devices. This is due to our slim design, which includes just a semicircular cross-section. Low relative tissue damage is an advantage of our design that adds to its potential feasibility in actual practice.

We are able to show that this device can successfully be used to steer through biological tissue. Specifically, it is able to perform turns in liver tissue, which is a potential target organ for steerable needle applications. Additionally, the turn radius for each device continues to be consistent with the turn radii outlined in the previous work and those described by tape spring theory [4]. Our small turn radius, the smallest of any device, means that a user would be able to have precise control, which practically means that adjustments to its trajectory can be made closer to the final target. These turn radii being consistent between gel phantoms and real tissue means that this navigational advantage would also apply to navigation in real tissues.

In future studies, we will explore using our steerable needle to perform multiple consecutive bends to form more complex paths. The effect of these paths on tissue damage could be quantified using the needle cast method. Additionally, the effect of payload delivery, such as biopsy devices, or drug injections should be evaluated for its effect on tissue damage.

Authors' Contributions: The authors confirm contribution to the paper as follows: study conception and design: O. Abdoun, M. Yim; data collection: O. Abdoun; analysis and interpretation of results: O. Abdoun, M. Yim; draft manuscript preparation: O. Abdoun, M. Yim. All authors reviewed the results and approved the final version of the manuscript.

Conflicts of Interest: The authors have no conflicts of interest.

Acknowledgment

The authors would like to thank Eza Koch and Elizabeth Tu for their work in early prototyping of this device.

References

[1] M. Scali, T. P. Pusch, P. Breedveld, and D. Dodou, "Needle-like instruments for steering through solid organs: A review of the scientific and patent literature," in *Proc. Inst. Mech. Engineers, Part H: J. Eng. Med.*, vol. 231, no. 3, pp. 250–265, 2017.

[2] M. Babaiasl, F. Yang, and J. P. Swensen, "Robotic needle steering: State-of-the-art and research challenges," *Intell. Serv. Robot.*, vol. 15, pp. 679–711, 2022.

[3] I. Elgezua, Y. Kobayashi, and M. G. Fujie, "Survey on current state-of-the-art in needle insertion robots: Open challenges for application in real surgery," *Procedia CIrP*, vol. 5, pp. 94–99, 2013.

[4] O. T. Abdoun and M. Yim, "A tape spring steerable needle capable of sharp turns," *bioRxiv*, 2023, doi: 10.1101/2023.05.04.539394.

[5] K. Seffen and S. Pellegrino, "Deployment of a rigid panel by tape-springs," Cambridge Univ. Dept. of Eng., Cambridge, U.K., Tech. Rep., Jul. 1997.

[6] T. K. Adebar, J. D. Greer, P. F. Laeseke, G. L. Hwang, and A. M. Okamura, "Methods for improving the curvature of steerable needles in biological tissue," *IEEE Trans. Biomed. Eng.*, vol. 63, no. 6, pp. 1167–1177, Jun. 2016.

[7] P. J. Swaney, J. Burgner, H. B. Gilbert, and R. J. Webster, "A flexure-based steerable needle: High curvature with reduced tissue damage," *IEEE Trans. Biomed. Eng.*, vol. 60, no. 4, pp. 906–909, Apr. 2013.

[8] A. Majewicz et al., "Behavior of tip-steerable needles in ex vivo and in vivo tissue," *IEEE Trans. Biomed. Eng.*, vol. 59, no. 10, pp. 2705–2715, Oct. 2012.

[9] A. Kemper, A. Santago, J. Stitzel, J. Sparks, and S. Duma, "Biomechanical response of human liver in tensile loading," *Ann. Adv. Automot. Med.*, vol. 54, pp. 15–26, 2010.

[10] F. Casanova, P. R. Carney, and M. Sarntinoranont, "Effect of needle insertion speed on tissue injury, stress, and backflow distribution for convection-enhanced delivery in the rat brain," *PLoS One*, vol. 9, no. 4, 2014, Art. no. e94919.

[11] Y. Koethe, S. Xu, G. Velusamy, B. J. Wood, and A. M. Venkatesan, "Accuracy and efficacy of percutaneous biopsy and ablation using robotic assistance under computed tomography guidance: A phantom study," *Eur. Radiol.*, vol. 3, no. 24, pp. 723–730, 2014.

[12] Y. Fukushima and K. Naemura, "Estimation of the friction force during the needle insertion using the disturbance observer and the recursive least square," *Robomech J.*, vol. 1, no. 1, pp. 1–8, 2014.